JBC Papers in Press. Published on December 2, 2020 as Manuscript RA120.015896
The latest version is at https://www.jbc.org/cgi/doi/10.1074/jbc.RA120.015896

YAP contributes to DNA methylation remodeling upon mouse embryonic stem cell differentiation

Fabiana Passaro[1]*, Ilaria De Martino[1], Federico Zambelli[2,3], Giorgia Di Benedetto[1], Matteo Barbato[1], Anna Maria D'Erchia[3,4], Caterina Manzari[3], Graziano Pesole[3,4], Margherita Mutarelli[5], Davide Cacchiarelli[5], Dario Antonini[6], Silvia Parisi[1], Tommaso Russo[1]*

[1]Department of Molecular medicine and medical biotechnology, University of Napoli Federico II, Italy
[2]Department of Biosciences, University of Milano, Italy
[3]Institute of Biomembranes, Bioenergetics and Molecular Biotechnologies, National Research Council, Italy
[4]Department of Biosciences, Biotechnology and Biopharmaceutics, University of Bari, Italy
[5]Tigem and Department of Translational Medicine, University of Napoli Federico II, Italy
[6]Department of Biology, University of Napoli Federico II, Italy

*Corresponding authors:
Fabiana Passaro, fabiana.passaro@unina.it
Tommaso Russo, tommaso.russo@unina.it

Running Title: YAP and DNA methylation in differentiating mouse ESCs

Keywords: yes-associated-protein YAP, DNA methyltransferases, Dnmt3l, Ephemeron, embryonic stem cells, epiblast-like stem cells, differentiation, pluripotency, stemness

Abstract

The Yes-associated protein YAP, one of the major effectors of the Hippo pathway together with its related protein TAZ, mediates a range of cellular processes from proliferation and death to morphogenesis. YAP and TAZ regulate a large number of target genes, acting as co-activators of DNA-binding transcription factors or as negative regulators of transcription by interacting with the nucleosome remodeling and histone deacetylase complexes. YAP is expressed in self-renewing embryonic stem cells (ESCs), although it is still debated whether it plays any crucial roles in the control of either stemness or differentiation. Here we show that the transient downregulation of YAP in mouse ESCs perturbs cellular homeostasis, leading to the inability to differentiate properly. Bisulfite genomic sequencing revealed that this transient knockdown caused a genome-wide alteration of the DNA methylation remodeling that takes place during the early steps of differentiation, suggesting that the phenotype we observed might be due to the dysregulation of some of the mechanisms involved in regulation of ESC exit from pluripotency. By gene expression analysis we identified two molecules which could have a role in the altered genome-wide methylation profile: the long non-coding RNA Ephemeron, whose rapid upregulation is crucial for ESCs transition into epiblast, and the methyltransferase-like protein Dnmt3l, which, during the embryo development, cooperates with Dnmt3a and Dnmt3b to contribute to the *de novo* DNA methylation that governs early steps of ESC differentiation. These data suggest a new role for YAP in the governance of the epigenetic dynamics of exit from pluripotency.

Introduction

One of the molecular machineries that play crucial roles during embryo development is that involving the Yes-associated protein YAP and the related protein TAZ (1,2). These two proteins play a fundamental role in the so-called Hippo pathway, as they, through a cytosol-nucleus shuttling regulated by nucleus-excluding phosphorylation, govern the transcription of various genes involved in sensing mechanical stress (3), cell proliferation and apoptosis (4,5), organ size (6). YAP and TAZ function as co-activators of the transcription factors TEADs (TEA/ATTS domain) (1), but the multitasking ability of YAP/TAZ is demonstrated by many results indicating TEAD-independent functions even outside the nucleus (7).

The critical role of these two proteins during the very early steps of development is recapitulated by the phenotype of YAP/TAZ double knock out: these embryos are arrested in the pre-morula stage (8), likely due to the induced repression of Sox2 preventing the appearance of the inner cell mass phenotype. At the morula stage, YAP is responsible for the activation of trophoblast master genes, like Cdx2, in the cells of the external layer, thus governing the acquisition of the trophoblast cell identity (9). Besides, YAP is expressed in the blastocyst and, *in vitro*, in embryonic stem cells (ESCs). Several works aimed at characterizing the function of YAP/TAZ in ESCs. Some results indicated that the suppression of YAP or TEAD resulted in the decreased intensity of AP staining of colonies and the downregulation of Oct4 and Sox2, with concomitant expression of differentiation markers, like T, AFP and Gata4 (10). Accordingly, overexpression of a TEAD dominant-negative protein led to the induction of ESC differentiation toward the endodermal lineage (11). *In vivo* analysis showed that high TEAD activity sustains pluripotency in the inner cells mass, while cells with low TEAD levels are eliminated (5). However, conflicting results showed that YAP/TAZ depletion had no effects on the stemness of ESCs grown in 2i medium and that, in these 2i conditions, YAP/TAZ downregulation mimics GSK3 inhibitor that blocks the β-catenin pathway (7). Consistent with these results, the silencing or the KO of YAP has no effects on the maintenance of the undifferentiated state (12). Furthermore, in differentiation-inducing conditions, YAP KD results in an insufficient accumulation of differentiation markers, like T, Gata6 and Gata3, although Oct4 and Nanog are normally suppressed (12).

These apparently conflicting results could at least in part depend on the multifaced activities of YAP/TAZ in the various steps of ESC differentiation, whose suppression in different experimental conditions could lead to diverse consequences. To address this point, we explored the effects of a very transient downregulation of YAP on the differentiation of mouse ESCs. We found that, although the normal YAP levels are completely rescued during the differentiation process, YAP KD cells show a genome methylation profile significantly different from

that of the control cells. Looking at the expression profile of undifferentiated YAP KD cells, we appreciated significant downregulation of Dnmt3l and the Ephemeron lncRNA. These findings indicate that YAP expression in undifferentiated ESCs is necessary to sustain the appropriate machinery responsible for the remodeling of the genome methylation patterns taking place at the exit of ESCs from the naïve state.

Results

Transient knockdown of YAP affects early steps of ESCs differentiation

We decided to explore the possible long-lasting effects of a transient YAP suppression in ESCs. To this aim, E14Tg2a clones, stably expressing GFP under control of the neural-specific promoter of the α1-tubulin gene (α1T-GFP) (13), were transiently transfected with a mixture of siRNAs eliciting a robust suppression of YAP expression (Supporting information Figure S1). 48 hours after transfection, YAP KD cells were induced to differentiate toward the neuroectodermal fate (13) and GFP expression was monitored at various time points during the differentiation process. As shown in Figure 1A, the number of GFP-positive cells was significantly decreased in YAP KD since the very first step of differentiation (day 4), with respect to control knockdown (CTR KD) cells, transiently transfected with siRNA Negative Control Duplex. Accordingly, at later stages (day 14) the differentiation process in YAP KD was incomplete, with a reduced number of cells expressing β3-tubulin (Figure 1B). The expression profile of late marker genes also confirmed that the transient KD of YAP severely affects neuroectodermal differentiation (Figure 1C).

The expression profile of YAP over differentiation steps confirmed the transiency of YAP silencing, as its mRNA and protein levels returned at steady state at day 4 of differentiation (Figure 1D and 1E). Nevertheless, the consequences of YAP suppression lasted until the end of the differentiation protocol, strongly suggesting that YAP could play a role in ESCs or in the early steps of their differentiation process and that this activity is determinant for the following events.

At this point, we explored the ability of YAP KD cells to differentiate toward the mesendodermal fate to address whether the transient downregulation of YAP expression in ESCs interferes specifically with the pathway of neuroectodermal differentiation or, instead, induces a general perturbation of the differentiation potential of ESCs. To this aim, we transiently transfected with YAP siRNAs the E14Tg2a clone MLC2v-GFP, in which the expression of GFP is under control of the cardiomyocyte-specific promoter of MLC2v gene (14). 48 hours after transfection, YAP KD cells were induced to differentiate into mesodermal derivatives by Embryoid Bodies (EBs) formation in mesodermal culture conditions (15). Again, 8 days after the induction of differentiation the number of GFP-positive cells was reduced in YAP KD cells (Figure 1F), and, interestingly, while cardiomyocyte colonies from CTR KD cells showed the expected beating phenotype, almost no beating areas were found in YAP KD cells (Figure 1G). These results suggest that the transient downregulation of YAP expression compromises the potential of undifferentiated ESCs to undertake differentiation properly.

Transient knockdown of YAP causes a perturbation of ESCs homeostasis

The partial inability of ESCs to undertake differentiation could be due, on the one hand, to premature loss of pluripotency or, on the contrary, to the persistence of stemness despite and after the induction of differentiation.

To explore whether YAP plays some role in the maintenance of the undifferentiated state of ESCs, we transiently silenced YAP expression in E14Tg2a cells by siRNAs or shRNAs (Supporting information Figure S2A). After 48 hours, KD cells were plated in the absence of LIF for a further 48 hours, and RNA samples were analyzed to measure the expression of stemness marker genes. The results shown in Figure 2A demonstrate that the expression profile of the main stemness markers was not affected by the transient silencing of YAP. These cells were also plated at low density and cultured for 7 more days in presence of LIF and serum to examine the formation of alkaline-phosphatase-positive (AP+) colonies. As shown in Figure 2B, both CTR and YAP KD cells were able to form AP+ colonies with a robust AP staining. However, a difference emerged in the total number of colonies derived from YAP KD cells, that was significantly lower than that of CTR KD (Figure 2B).

FACS analysis showed a certain degree of cell death 48 hours after YAP silencing (Figure 2C), but not so high to support the possibility that the observed decreased number of AP colonies and differentiated cells were exclusively due to cell death.

To assess YAP KD cell viability during the early steps of differentiation, YAP KD cells were induced to differentiate toward neuroectodermal fate by Serum Free Embryoid Bodies (SFEBs) formation (15). Trypan Blue exclusion assay showed an increased number of non-vital cells among those in YAP KD SFEBs with respect to CTR KD SFEBs (Figure 2D), which were probably responsible for the differences in SFEBs size as assessed by measuring SFEBs diameter (Figure 2E), with YAP KD SFEBs appearing smaller than CTR KD SFEBs.

All together, these results suggest that transient YAP silencing in undifferentiated ESCs causes a perturbation of cellular homeostasis leading to a reduced survival of cells. The latter can in part explain the decrease in the number of total cells when they are re-plated to examine self-renewal or differentiation. Nevertheless, surviving cells seem to be unable to differentiate properly, suggesting that the transient downregulation of YAP stably affect the signature of selected subpopulations of surviving cells.

Bisulfite genomic sequencing reveals a general perturbation in the methylation pattern of YAP KD cells upon differentiation.

The phenotypes induced by the transient suppression of YAP are likely due to events that continue to exert their effects also after normal levels of YAP expression are restored. One possibility is that transient YAP silencing could be responsible for deregulation in genome-wide *de novo* methylation, which is known to take place upon the induction of ESC differentiation (16,17). To explore this possibility, we analyzed by BS-seq the methylation pattern of CTR and YAP KD cell in undifferentiated ESCs (T0) vs cells differentiated as SFEBs (T4). First of all, we analyzed the changes in genomic DNA methylation occurring in CTR cells upon 4 days of differentiation, compared to CTR cells at T0, finding 6661 Differential Methylated Regions (DMRs) with a q-value $\leq$ 0.05 (Supporting information Table S1). Then, we performed the same analysis in YAP KD cell at T4 SFEBs with respect to T0, identifying 6898 DMRs (Supporting information Table S1). Although the number of DMRs was similar in absolute terms between the two conditions, the transient suppression of YAP had a dramatic effect on genome methylation. As shown in Figure 3A, about 30% of the 6661 DMRs observed in the differentiation of CTR cells led to a gain of methylation, compared to only 13% gain of methylation in the 6898 DMRs observed in YAP KD cells, while, on the other hand, most of the DMRs observed in YAP KD cells were loss of methylation (86.9% vs 69.8% in CTR cells), with some chromosomes particularly affected, as in the cases of chromosomes 1, 2, 3, 4, 13 and 14 (Figure 3B).

We then examined the loci showing differences between CTR and YAP KD cells and in particular the loci with differentiation-dependent loss of methylation in YAP KD cells and not in CTR cells and gain of methylation in CTR cells and not in YAP KD cells (Supporting information Table S1). Considering DMRs with a q-value of at least 0.05, there are 2325 loci where the loss of methylation was evident only in YAP KD cells and not in CTR cells and 1218 loci where, on the contrary, there is a gain of methylation in CTR cells and not in YAP KD cells. We retrieved the sets of genes closest to the DMRs and analyzed them by using the PANTHER gene ontology platform (18). Interestingly, we observed very significant overrepresentation of the Wnt signaling pathway, and the related Cadherin pathway, for those genes where the loss of methylation emerged only in YAP KD cells (Figure 3C).

These data demonstrated that the transient downregulation of YAP affects the repatterning of *de novo* methylation occurring in the very early steps of ESCs differentiation. This might ultimately lead to the lack of appropriate governance of the epigenetic dynamics occurring at the exit from pluripotency.

Gene expression profile of YAP KD cells reveals a signature related to *de novo* DNA methylation

Considering that the phenotype we observed is caused by a transient downregulation of YAP, we decided to look at the expression profiles of ESCs 48 hours after the transfection with YAP siRNAs, when YAP reaches the minimum levels. Total RNA was isolated from three independent samples each for YAP KD and CTR KD and analyzed by RNA-Seq. As shown in Figure 4A, the expression of 1196 genes was significantly deregulated in YAP KD cells ($p<0.005$, FDR<0.05), with 54% of which resulted downregulated (Supporting information Table S2). In parallel, we also analyzed the gene expression profile of ESCs transfected with a YAP encoding vector (OE YAP) or with the empty vector (OE CTR) (Figure 4B), again using three independent biological samples. In this case,

488 transcripts were found overexpressed (73%) or underexpressed (27%), as a consequence of YAP ectopic expression (Supporting information Table S2 and Supporting information Figure S3).
The comparison between the KD and OE data sets showed that 215 genes were common to both sets, with 134 coherently downregulated in YAP KD cells and upregulated in YAP OE cells, and 46 showing the opposite behavior (Figure 4C).
Panther analysis of the most deregulated genes (0.6<FC>1.7) in YAP KD cells revealed a statistically significant enrichment (FDR<0.05) in GO terms related to development and morphogenesis (Figure 4D).
Among the genes downregulated upon YAP KD and upregulated in YAP OE cells, we focused our attention on two genes that could have a role in the altered genome-wide methylation profile we observed in YAP KD cells. The first one is Ephemeron (Eprn - D630045M09Rik), which encodes a lncRNA that modulates the dynamics of exit from naïve pluripotency (19). Indeed, it was recently described that Eprn is expressed in undifferentiated mouse ESCs and its rapid upregulation is crucial for ESCs transition into Epiblast (19). Upon removal of 2i and LIF, Eprn deletion delays the extinction of ESC identity by reducing Lin28a expression, with the consequent persistence of let-7 microRNAs. In parallel, the upregulation of *de novo* methyltransferases Dnmt3a/b is delayed, which retards ES cell transition (19). Accordingly, our expression profile of YAP KD cells showed a slight but significant (p=0.0042) decrease of Lin28a (Supporting information Table S2). We first confirmed that, in our experimental conditions, Eprn was significantly downregulated in undifferentiated ESCs (Figure 5A). We also observed that, while Eprn was induced in CTR cells 12 hours after LIF removal, this induction was abolished entirely in YAP KD cells (Figure 5B). In addition, the expression profiles of Lin28a and Lin28b, following LIF withdrawal, were altered in YAP KD cells, with an evident downregulation of Lin28a at T12 and of Lin28b at T48. Although not statistically significant, we observed lower mRNA levels also for Dnmt3a and Dnmt3b in YAP KD cells vs CTR cells (Figure 5B).
Although RNA-seq data and qPCR assays did not show significant changes in the expression of Dnmt3a or b, we found that their activating co-factor, Dnmt3l, was downregulated upon YAP KD and upregulated in YAP OE cells. Dnmt3l encodes a protein that, although lacking enzyme activity, cooperates during the embryo development with Dnmt3a and Dnmt3b, contributing to the *de novo* DNA methylation that governs the early steps of ESC differentiation (20). Of interest, Dnmt3l is also expressed in undifferentiated ESCs (21) where it hampers the methylation of bivalent gene promoters by interacting with the PRC2 complex (22). We confirmed by qPCR that Dnmt3l was downregulated in ESCs by YAP KD and upregulated upon YAP OE (Figure 5A). Accordingly, Dnmt3l protein was significantly decreased in YAP KD cells (Figure 5C).
As in the case of Eprn, the expression of Dnmt3l was induced 12 hours after LIF withdrawal. However, this induction is not observed in YAP KD cells, where Dnmt3l levels remained very low during all the differentiation process (Figure 5D).

Eprn gene is a direct target of TEAD/YAP is ESCs

We addressed the question of whether Dnmt3l and/or Eprn are direct targets of YAP. In the experimental conditions we explored, the fraction of ESCs where YAP is clearly present in the nucleus is relatively low (about 20%), while nuclear YAP is undetectable in most, if not all, the cells upon the induction to differentiation (Supporting information Figure S4A and S4B). Thus, most of the nuclear effects of transient YAP KD should take place in the undifferentiated cells and/or in the very early steps of differentiation. To address this point, ChIP-seq experiments for YAP were run in duplicate in undifferentiated ESCs. We identified 428 bona fide peaks (Supporting information Table S3) whose TSS is located within 500 kbps from the peaks (Supporting information Figure S5A and Supporting information Table S3). Gene Ontology analysis revealed that putative target genes could be significantly clustered based on biological functions associated with epigenetic regulation of gene expression, chromatin silencing, chromatin assembly and disassembly (Supporting information Figure S5B).
By crossing ChIP-seq with RNA-seq data, we found 43 putative direct targets (Figure 6A), which were deregulated by YAP KD or OE and located in the proximity (500kbps) of significant ChIP peaks. Neither Dnmt3l nor Eprn genes showed significant peaks in the proximity of their TSS. However, relaxing the stringency threshold, we identified a peak in the second intron of Eprn gene (Supporting information Figure S6A).

154 out of 428 peaks from our data correspond to TEAD peaks present in published ChIP-seq collections (23) (Supporting information Table S4), thus we decided to examine whether TEAD transcription factors could interact with YAP in the direct binding to the Epnr gene by ChIP-assay, upon silencing of either TEAD1 or TEAD2 (Supporting information Figures S5C). As shown in Figure 6B, we confirmed the binding of YAP to the peak in the second intron of Eprn gene. Moreover, the comparison between the amount of DNA immunoprecipitated in TEADs KD samples with respect to CTR KD revealed that this binding was TEAD- dependent. The interaction between YAP and TEADs was confirmed also for a subset of selected peaks from our ChIP-seq (Supporting information Figure S6B).

Dnmt3l and Eprn transient knockdown affect ESCs differentiation.

In order to define the contribution of Dnmt3l and Eprn to the phenotype induced by YAP downregulation, α1T-GFP cells were transiently transfected with siRNAs producing a robust suppression of YAP, Dnmt3l or Eprn expression (Supporting information Figure S7A). Two independent siRNAs for each target gene were used. Then, 48 hours after transfection, KD cells were induced to differentiate toward the neuroectodermal fate. As shown in Figure 7A, both Dnmt3l and Eprn transient suppression lead to a phenotype similar to that induced by YAP downregulation, indeed showing decreased number of cells expressing β3-tubulin at final stage of differentiation. Accordingly, the expression profile of late neural marker genes also confirmed that the downregulation of Dnmt3l or Eprn expression severely affects neuroectodermal differentiation (Figure 7B).

To explore the possibility that the forced expression of a single YAP target could be sufficient to rescue the YAP KD phenotype, we cloned the coding sequence of mouse Dnmt3l gene into the pCAG-3xflag vector (13) in order to over-express the methyltransferase in YAP KD α1T-GFP cells (Supporting information Figure S7A). 48 hours after transfection, cells were seeded in neuroectodermal differentiation conditions to investigate the effects of Dnmt3l over-expression on neuroectodermal differentiation ether in CTR KD or YAP KD cells. By the evaluation of β3-tubulin expressing cells at final stage of differentiation, we found that no significant recovery of differentiation functions affected by YAP KD could be obtained by the sole forced expression of Dnmt3L (Supplementary information Figure S7B). Accordingly, the expression profile of late marker genes resulted comparable in YAP KD cells, with or without Dnmt3l over-expression (Supplementary information Figure S7C).

Discussion

Here we show results indicating that YAP is required in ESCs to allow them to undergo the epigenetic changes that are necessary for the exit from the undifferentiated state. Indeed, we observed that transient downregulation of YAP affects the changes in the DNA methylation pattern between undifferentiated and differentiated mouse ESCs. This phenotype is characterized by a significant increase in the proportion of regions where methylation is lost and a concomitant decrease in the proportion of regions where *de novo* methylation occurs. In particular, we observed that there are many loci that, upon the exit from pluripotency state, were significantly losing DNA methylation only in YAP KD cells, and that, on the other hand, there are numerous loci where a gain of methylation was only observed in CTR cells. These observations support the conclusion that transient suppression of YAP in ESCs leads to a dysregulation of DNA methylation in terms of both a defect in *de novo* methylation and an excess of demethylation. These phenomena appear to be rather specific, because of the very high degree of inappropriate demethylation or lack of *de novo* methylation at specific loci. This observation is further supported by the overrepresentation of genes involved in the Wnt signaling pathway associated with the DMRs. It is worth noting that we observed that more than 20% of genes whose expression is modified as a consequence of transient YAP KD are also putative direct targets of Tcf3 (24). The cross-talk between YAP/TAZ and the Wnt pathway was reported several years ago (25). Indeed, YAP/TAZ regulate, in a transcription-independent fashion, the Wnt pathway by favoring the degradation of β-catenin (7). Our observations point to a possible second YAP-dependent mechanism to regulate the Wnt signaling, based on the methylation, and in turn suppression, of several Wnt-related genes. On the basis of our results, it cannot be excluded that TAZ could contribute to the YAP-dependent mechanisms.

By analyzing the expression profile of ESCs where YAP was transiently downregulated, we realized that this phenotype could be, at least in

part, explained by the YAP KD-dependent downregulation of Dnmt3l and the lncRNA Eprn. Dnmt3l is similar to the two *de novo* DNA methyltransferases Dnmt3a and Dnmt3b, but it lacks the catalytic activity (26). Numerous results indicated that this protein could function as an accessory factor to Dnmt3a and Dnmt3b. Indeed, it interacts with the catalytically competent methyltransferases, increases their activity at least *in vitro* (27), and stabilizes them as in the case of the Dnmt3a2 isoform (21). Dnmt3l interaction with Dnmt3a was characterized by analyzing the crystal structure of the complex confirming the formation of a tetramer including two Dnmt3l subunits, each interacting with Dnmt3a through their C-terminal domains (28). This structure is compatible with the binding of the N-terminal ADD domain of Dnmt3l with unmethylated lysine 4 of histone H3, that could favor the targeting of catalytically competent methyltransferases to specific chromatin domains (29). Furthermore, Dnmt3l also interacts with Ezr2, a subunit of the polycomb complex PRC2 and this results in the protection of bivalent gene promoters from *de novo* methylation by Dnmt3a and Dnmt3b, thus keeping them competent for the following activation as part of specific differentiation programs (22). Although Dnmt3l KO mice have no defects at birth, they are sterile showing a clear germline phenotype, thus indicating that Dnmt3l could be necessary for Dnmt3a-dependent methylation in gametogenesis (21). However, Dnmt3a deficiency is accompanied by undermethylation of DNA in the early steps of embryo development (21-30,31). Our results clearly indicate that Dnmt3l downregulation induced a phenotype similar to that observed in YAP KD cells. However, its overexpression in YAP KD cells failed to rescue the normal phenotype, thus indicating that there are other genes, whose expression is affected by YAP transient downregulation that contribute to the genesis of the observed phenotype.

Another gene whose behavior was altered in YAP KD cells is that transcribing for Eprn, a mouse-specific lncRNA. It was observed that Eprn is transiently upregulated upon the exit of ESCs from naïve pluripotency and its suppression, by either gene knock-out or RNAi, was accompanied by a delayed downregulation of pluripotency-associated genes (19). One of the phenotypes found in Eprn KO cells is reduced methylation at the Nanog gene promoter, that mimics the decreased methylation observed in Dnmt3a/b gene KO cells (19). Thus, on the basis of our results, it is possible that in YAP KD ESCs the decreased basal levels of Eprn and the absence of any Epnr induction upon ESC differentiation (see Figure 5B) have a negative effect upon the *de novo* genome methylation. Mammalian genomes produce thousands of lncRNAs, but their functions are in most cases still not definitively addressed. Numerous lncRNAs have regulatory roles in ESC (32), and many of them have a role in the regulation of the Hippo pathway (33). Less is known about the possible regulation of lncRNA gene expression by the Hippo pathway.

While we demonstrated that the transcription of Eprn gene is under the control of YAP, which binds to a *cis* element is the second intron of the gene and that this binding is dependent on TEAD1/2, the mechanisms through which YAP downregulation causes a decrease of Dnmt3l could be indirect. The ChIP-seq of YAP in undifferentiated ESCs showed a relatively small number of significant peaks, likely because the relatively small fraction of undifferentiated ESCs where YAP is robustly expressed in the nucleus. As expected, we found numerous deregulated genes of well-known YAP direct targets, such as Cyr61, GADD45a, Wwc2 (for a complete list see Supporting information Table S2). Our ChIP-seq assays did not show any evidence of binding of YAP in the proximity of Dnmt3l gene, so it is conceivable that its downregulation in YAP KD depends on an indirect mechanism, acting either at mRNA level and/or at protein level. TargetScan (34) did not find any conserved miRNA binding sites in the 3'UTR of Dnmt3l, but of course this does not exclude the possibility that Dnmt3l suppression was dependent on a miR-dependent mechanism.

Experimental Procedures

Cell Culture and Transfection

E14Tg2a (BayGenomics) mouse ESCs were maintained on feeder-free, gelatine-coated plates in the following ESC medium: Glasgow minimum essential medium (Sigma) supplemented with 2 mM glutamine, 1 mM sodium pyruvate, 1X non-essential amino acids (all from Thermo Fisher Scientific), 0.1 mM β-mercaptoethanol (Sigma), 10% fetal bovine serum (HyClone Laboratories), and 10^3 U/ml leukaemia inhibitory factor (Merck). Generation and culture of the α1tub-GFP and of the Mlc2v-GFP cell lines have been described previously (13,14).

The pCAG-mYAP vector was generated by cloning the coding sequence of wt mouse YAP

(from bac clone n°: MR226049-Origene) into the pCAG vector (13).
The pCAG-3xflag-mDnmt3L was generated by cloning the coding sequence of wt mouse DNMT3L (from pMX-Dnmt3l vector – Addgene) into the pCAG-3xflag vector (13). Transfections of small interfering RNAs, shRNAs, pCAG-mYAP and pCAG-3xflag-Dnmt3L plasmids were performed using Lipofectamine 2000 (Thermo Fisher Scientific) following the manufacturer's instructions. shRNAs form Mouse pSM2 retroviral shRNAmir library (Open Biosystems) were: 5'-TGC TGT TGA CAG TGA GCG AGC AGA CAG ATT CCT TTG TTA ATA GTG AAG CCA CAG ATG TAT TAA CAA AGG AAT CTG TC T GCG TGC CTA CTG CCT CGG A-3' for YAP knockdown; 5'-TGC TGT TGA CAG TGA GCG CTC GCT TGG GCG AGA GTA ATA GTG AAG CCA CAG ATG TAT TAC TCT CGC CCA AG CGA GTT GCG TGC CTA CTG CCT CGG A-3' for CONTROL (non silencing) knockdown
Stealth siRNAs (Thermo Fisher Scientific; Cat No./ID: 1320001) were: MSS238823 and MSS238824 for YAP; MSS211217 and MSS211218 for TEAD1; MSS278118 and MSS278119 for TEAD2; MSS244161 and MSS285157 for DNMT3L. FlexiTube siRNAs (Qiagen; Cat No./ID: 1027417) for EPRN knockdown were: SI05681977 and SI05681984. Stealth siRNA Negative Control Med GC Duplex (Thermo Fisher Scientific; Cat No./ID: 12935112 and 12935113) were used for negative controls.

Alkaline phosphatase staining, neuroectodermal and mesodermal differentiation

For alkaline phosphatase staining, ESCs were cultured at clonal density (30 cells/cm2). Cells were fixed in 10% cold neutral formalin buffer (10% formalin, 110 mM Na2HPO4, 30 mM NaH 2PO4 H2O) for 15 min and then rinsed in distilled water for 15 min. The staining was obtained by incubation for 45 min at room temperature with the following staining solution: 0.1 M Tris·HCl, 0.01% naphthol AS MX-PO4 (Sigma), 0.4% N, N-dimethylformamide (Sigma), 0.06% red violet LB salt (Sigma).
For neuroectodermal differentiation, ESCs were induced to differentiate either in monolayer (13), by placing 3 x 10^3 ESCs per cm^2 in cell gelatine-coated cell culture plates, or by SFEBs formation (15), by placing 1 x 10^6 ESCs in 100 mm petri dishes, in the following differentiation medium: Glasgow minimum essential medium supplemented with 2 mM glutamine, 1 mM sodium pyruvate, 1X non-essential amino acids, 0.1 mM β-mercaptoethanol, and 10% KO serum replacement (Thermo Fisher Scientific). SFEBs indicate aggregates at 4 days (T4) of ESC differentiation unless noted otherwise.
ESC differentiation into mesoderm was induced by Embryoid bodies (EBs) formation and have been described previously (15).

RNA isolation, reverse transcription and quantitative PCR

Quantitative PCR (qPCR) have been previously described (35). In brief, total RNA was extracted by TriSure (Bioline), and first-strand cDNA was synthesized using Mu-MLV RT (New England BioLabs) according to the manufacturer's instructions. qPCR was carried out with the QuantStudio 7 Flex (Thermo Fisher Scientific) using Fast SYBR Green PCR Master Mix (Thermo Fisher Scientific). The housekeeping ACTIN mRNA was used as an internal standard for normalization. Gene-specific primers used for amplification are listed in Supporting information Table S5. qPCR data are presented as fold changes relative to the indicated reference sample. mRNA expression levels were analysed performing a comparative analysis using $2^{-\Delta\Delta Ct}$.

Antibodies and Western blot analysis

Undifferentiated and differentiated ESCs were lysed in RIPA buffer containing 150 mM sodium chloride, 1% NP-40, 0.5% sodium deoxycholate, 0.1% SDS (sodium dodecyl sulphate), 50 mM Tris, pH 8.0 and protease inhibitor cocktail (Sigma-Aldrich), and analysed by Western blot. The following primary antibodies were used: rabbit anti-Yap (1:1000; D8H1X Cell Signalling), rabbit anti-Dnmt3l (1:1000; E1Y7Q Cell Signalling), mouse anti-Vinculin (1:1000; G11 Santa Cruz Biotechnology), mouse anti-Flag (1:2000; Sigma). Western blots were developed with an ECL system (BioRad) using the following horseradish peroxidase–conjugated antibodies: anti-rabbit IgG (1:10,000), anti-mouse IgG (1:5000; both from Amersham Pharmacia Biotech).

Fluorescence-activated cell sorting analysis

Analysis of DNA content by propidium iodide (PI) incorporation to evaluate cell death was performed in permeabilized cells by flow cytometry. ESCs were dissociated and collected, washed in PBS, and resuspended in a solution containing 0.1% sodium citrate w/v, 0.1%

TritonX-100 v/v, and 50 mg/ml PI (Sigma). After incubation at 4°C for 30 min in the dark, cell nuclei were analyzed with a Fluorescence-Activated Cell Sorting (FACS) Accuri C6 (Becton Dickinson). Cellular debris was excluded from the analysis by raising the forward scatter threshold, the DNA content of the nuclei was registered on a logarithmic scale, and the percentage of the elements in the hypodiploid region was calculated.

Immunostaining and microscopy

For immunofluorescence analysis, ESCs were fixed, permeabilized, and incubated with primary antibodies and an appropriate secondary antibody (13). Nuclei were counterstained with DAPI (1:5000; Calbiochem). Sectioned SFEBs were obtained and stained as previously described (15). The following primary antibodies were used: anti-Yap (1:300; NB110-58358 Novus Biological), anti-βIII Tubulin (1:400; Sigma). Alexa Fluor 594 or 488 secondary antibodies were used (1:400; Thermo Fisher Scientific). Cells were visualized using an inverted microscope (Leica Microsystems), and the images were captured with a digital camera (DFC365 FX; Leica Microsystems) using LAS-AF software (Leica Microsystems).

Confocal images were acquired with LSM510META microscope (Carl Zeiss GmbH) using LSM510 software (Zeiss). After acquisition, the images were colour corrected using the brightness, contrast, and colour-balance commands applied to every pixel in each image.

RNA sequencing and analysis

Total RNAs from three independent samples each for YAP KD, CTR KD, YAP OE and CTR OE were extracted by TriSure (Bioline) and subjected to high-throughput sequencing with Illumina Genome Analyzer platform (Illumina). Reads have been mapped using STAR (36) on the mm10 reference genome using standard parameters. The RefSeq curated transcripts annotation downloaded from the UCSC Genome Browser database (37) was used as a reference to quantify expression through RSEM (38). Differential expression analysis was carried out using the edgeR package (39).

Chromatin immunoprecipitation

For ChIP-seq analysis, ESCs were cross-linked with 1% formaldehyde for 10 min at room temperature, and formaldehyde was then inactivated by the addition of 125 mM glycine. Cells were lysed and the chromatin was sonicated to an average DNA fragment length of 200 to 500 bp. Soluble chromatin extracts were immunoprecipitated using the rabbit polyclonal anti-Yap (NB110-58358 Novus Biological) or rabbit IgG (Abcam) as control. ChIP-seq library preparation was obtained by using the TruSeq ChIP Sample Prep Kit (Illumina) Then samples from two independent experiments were subjected to high-throughput sequencing with Illumina Genome Analyzer platform (Illumina). ChIP-Seq data were processed by Galaxy tools (40). Briefly, reads were mapped against the Mus musculus genome (UCSC, mm9) using bowtie software (version 0.9.9.1) with parameters -v 2 -a -m 100, tracking up to hundred best alignment positions per read and allowing at most two mismatches. Each alignment was weighted by the inverse of the number of hits. All quantifications were based on weighted alignments. Clusters of ChIP-Seq read alignments were identified employing MACS software (v.1.3.7.1). For ChIP-qPCR, samples were prepared as previously described (41). Supernatant obtained without antibody was used as an input control. qPCR analyses were performed by using the QuantStudio 7 Flex (Thermo Fisher Scientific) and Fast SYBR Green PCR Master Mix (Thermo Fisher Scientific). Primers used for ChIP-qPCR are listed in Supporting information Table S5. The amount of precipitated DNA was calculated relative to the total input chromatin and expressed as the fold enrichment relative to total input according to the following formula: fold enrichment = 2{Delta}Ct × 10, where {Delta}Ct = Ct(input) - Ct(immunoprecipitation), where Ct refers to cycle threshold.

BS-sequencing and analysis

Genomic DNA from two independent experiments each for YAP KD T0, YAP KD T4, CTR KD T0 and CTR KD T4 was extracted and purified by QIAamp DNA Kit (QIAGEN) according to the manufacturer's instructions. Reads have been quality trimmed using Trim Galore 0.6.5 (http://www.bioinformatics.babraham.ac.uk/projects/trim_galore/). Trimmed reads have been mapped on the mm9 reference genome (after in silico bisulphite conversion) using the BS-Seq alignment function of Bismark (42) with default options. Calling of methylated cytosines has been made using the methylation extractor utility of Bismark. Differential methylated regions (DMRs) have been identified by means of the methylKit R

package (43) using a tiling window of length 250bp and step 125bp. The window size was set to 250bp since this value is close to the median length (240bp) of the SureSelectXT Methyl-Seq Target Enrichment regions. Positions covered by less than six reads were excluded from the analysis. DMRs have been annotated using the genomation R package (44) on the mm9 RefSeq gene annotation downloaded from the UCSC Genome Browser database (38).

Statistical analysis

The number of biological replicates of each experiment is indicated in the figure legends. The means of at least 2 independent experiments were used to calculate SEM or SD and to perform statistical analysis (when appropriate). All P values were calculated by Student's T test, using a 2-tailed test and paired samples.

Data availability

All sequencing data have been deposited in the public repository GEO database (GSE157707).

Author contributions

FP and TR designed the project and the experiments, analyzed the results and wrote the paper, FP, IDM, GDB, MP, SP performed the experiments and analyzed results, FZ, GP, AMD, CM and DA performed and analyzed BS-seq, RNA-seq and ChIP-seq, DC and MM performed and analyzed ChIP-seq.

Funding and additional information

This work has been supported by grants from PRIN grants to TR and SP, Federico II FRA project to FP, "Prodotti alimentari" project from Regione Campania and PROCAN project from Italian Ministry of Research.

Conflict of interest

The authors declare that they have no conflicts of interest with the contents of this article.

References

1. Pocaterra, A., Romani, P., & Dupont, S. (2020). YAP/TAZ functions and their regulation at a glance. Journal of cell science, 133(2), jcs230425. https://doi.org/10.1242/jcs.230425
2. Moya, I. M., & Halder, G. (2019). Hippo-YAP/TAZ signalling in organ regeneration and regenerative medicine. Nature reviews. Molecular cell biology, 20(4), 211–226. https://doi.org/10.1038/s41580-018-0086-y
3. Dupont, S., Morsut, L., Aragona, M., Enzo, E., Giulitti, S., Cordenonsi, M., Zanconato, F., Le Digabel, J., Forcato, M., Bicciato, S., Elvassore, N., & Piccolo, S. (2011). Role of YAP/TAZ in mechanotransduction. Nature, 474(7350), 179–183. https://doi.org/10.1038/nature10137
4. Ma, S., Meng, Z., Chen, R., & Guan, K. L. (2019). The Hippo Pathway: Biology and Pathophysiology. Annual review of biochemistry, 88, 577–604. https://doi.org/10.1146/annurev-biochem-013118-111829
5. Hashimoto, M., & Sasaki, H. (2019). Epiblast Formation by TEAD-YAP-Dependent Expression of Pluripotency Factors and Competitive Elimination of Unspecified Cells. Developmental cell, 50(2), 139–154.e5. https://doi.org/10.1016/j.devcel.2019.05.024
6. Varelas X. (2014). The Hippo pathway effectors TAZ and YAP in development, homeostasis and disease. Development (Cambridge, England), 141(8), 1614–1626. https://doi.org/10.1242/dev.102376
7. Azzolin, L., Panciera, T., Soligo, S., Enzo, E., Bicciato, S., Dupont, S., Bresolin, S., Frasson, C., Basso, G., Guzzardo, V., Fassina, A., Cordenonsi, M., & Piccolo, S. (2014). YAP/TAZ incorporation in the β-catenin destruction complex orchestrates the Wnt response. Cell, 158(1), 157–170. https://doi.org/10.1016/j.cell.2014.06.013
8. Sasaki H. (2017). Roles and regulations of Hippo signaling during preimplantation mouse development. Development, growth & differentiation, 59(1), 12–20. https://doi.org/10.1111/dgd.12335
9. Nishioka, N., Inoue, K., Adachi, K., Kiyonari, H., Ota, M., Ralston, A., Yabuta, N., Hirahara, S., Stephenson, R. O., Ogonuki, N., Makita, R., Kurihara, H., Morin-Kensicki, E. M., Nojima, H., Rossant, J., Nakao, K., Niwa, H., & Sasaki, H. (2009). The Hippo signaling pathway components Lats and Yap pattern Tead4 activity to distinguish mouse trophectoderm from inner cell mass. Developmental cell, 16(3), 398–410. https://doi.org/10.1016/j.devcel.2009.02.003

10. Lian, I., Kim, J., Okazawa, H., Zhao, J., Zhao, B., Yu, J., Chinnaiyan, A., Israel, M. A., Goldstein, L. S., Abujarour, R., Ding, S., & Guan, K. L. (2010). The role of YAP transcription coactivator in regulating stem cell self-renewal and differentiation. Genes & development, 24(11), 1106–1118. https://doi.org/10.1101/gad.1903310
11. Tamm, C., Böwer, N., & Annerén, C. (2011). Regulation of mouse embryonic stem cell self-renewal by a Yes-YAP-TEAD2 signaling pathway downstream of LIF. Journal of cell science, 124(Pt 7), 1136–1144. https://doi.org/10.1242/jcs.075796
12. Chung, H., Lee, B. K., Uprety, N., Shen, W., Lee, J., & Kim, J. (2016). Yap1 is dispensable for self-renewal but required for proper differentiation of mouse embryonic stem (ES) cells. EMBO reports, 17(4), 519–529. https://doi.org/10.15252/embr.201540933
13. Parisi, S., Passaro, F., Aloia, L., Manabe, I., Nagai, R., Pastore, L., & Russo, T. (2008). Klf5 is involved in self-renewal of mouse embryonic stem cells. Journal of cell science, 121(Pt 16), 2629–2634. https://doi.org/10.1242/jcs.027599
14. Testa, G., Tarantino, C., Parisi, S., Galizia, G., Passaro, F., Della-Morte, D., Abete, P., Rengo, F., Salvatore, F., & Pastore, L. (2011). Serum withdrawal after embryoid body formation does not impair cardiomyocyte development from mouse embryonic stem cells. Cytotherapy, 13(3), 350–356. https://doi.org/10.3109/14653249.2010.520311
15. Navarra, A., Musto, A., Gargiulo, A., Petrosino, G., Pierantoni, G. M., Fusco, A., Russo, T., & Parisi, S. (2016). Hmga2 is necessary for Otx2-dependent exit of embryonic stem cells from the pluripotent ground state. BMC biology, 14, 24. https://doi.org/10.1186/s12915-016-0246-5
16. Petell, C. J., Alabdi, L., He, M., San Miguel, P., Rose, R., & Gowher, H. (2016). An epigenetic switch regulates de novo DNA methylation at a subset of pluripotency gene enhancers during embryonic stem cell differentiation. Nucleic acids research, 44(16), 7605–7617. https://doi.org/10.1093/nar/gkw426.
17. Auclair, G., Guibert, S., Bender, A., & Weber, M. (2014). Ontogeny of CpG island methylation and specificity of DNMT3 methyltransferases during embryonic development in the mouse. Genome biology, 15(12), 545. https://doi.org/10.1186/s13059-014-0545-5.
18. Mi, H., Muruganujan, A., Huang, X., Ebert, D., Mills, C., Guo, X., & Thomas, P. D. (2019). Protocol Update for large-scale genome and gene function analysis with the PANTHER classification system (v.14.0). Nature protocols, 14(3), 703–721. https://doi.org/10.1038/s41596-019-0128-8.
19. Li, M. A., Amaral, P. P., Cheung, P., Bergmann, J. H., Kinoshita, M., Kalkan, T., Ralser, M., Robson, S., von Meyenn, F., Paramor, M., Yang, F., Chen, C., Nichols, J., Spector, D. L., Kouzarides, T., He, L., & Smith, A. (2017). A lncRNA fine tunes the dynamics of a cell state transition involving Lin28, let-7 and de novo DNA methylation. eLife, 6, e23468. https://doi.org/10.7554/eLife.23468.
20. Borgel, J., Guibert, S., Li, Y., Chiba, H., Schübeler, D., Sasaki, H., Forné, T., & Weber, M. (2010). Targets and dynamics of promoter DNA methylation during early mouse development. Nature genetics, 42(12), 1093–1100. https://doi.org/10.1038/ng.708.
21. Veland, N., Lu, Y., Hardikar, S., Gaddis, S., Zeng, Y., Liu, B., Estecio, M. R., Takata, Y., Lin, K., Tomida, M. W., Shen, J., Saha, D., Gowher, H., Zhao, H., & Chen, T. (2019). DNMT3L facilitates DNA methylation partly by maintaining DNMT3A stability in mouse embryonic stem cells. Nucleic acids research, 47(1), 152–167. https://doi.org/10.1093/nar/gky947.
22. Neri, F., Krepelova, A., Incarnato, D., Maldotti, M., Parlato, C., Galvagni, F., Matarese, F., Stunnenberg, H. G., & Oliviero, S. (2013). Dnmt3L antagonizes DNA methylation at bivalent promoters and favors DNA methylation at gene bodies in ESCs. Cell, 155(1), 121–134. https://doi.org/10.1016/j.cell.2013.08.056.
23. Croci, O., De Fazio, S., Biagioni, F., Donato, E., Caganova, M., Curti, L., Doni, M., Sberna, S., Aldeghi, D., Biancotto, C., Verrecchia, A., Olivero, D., Amati, B., & Campaner, S. (2017). Transcriptional integration of mitogenic and mechanical signals by Myc and YAP. Genes & development, 31(20), 2017–2022. https://doi.org/10.1101/gad.301184.117.
24. Cole, M. F., Johnstone, S. E., Newman, J. J., Kagey, M. H., & Young, R. A. (2008). Tcf3 is an integral component of the core regulatory circuitry of embryonic stem cells. Genes & development, 22(6), 746–755. https://doi.org/10.1101/gad.1642408.

25. Varelas, X., Miller, B. W., Sopko, R., Song, S., Gregorieff, A., Fellouse, F. A., Sakuma, R., Pawson, T., Hunziker, W., McNeill, H., Wrana, J. L., & Attisano, L. (2010). The Hippo pathway regulates Wnt/beta-catenin signaling. Developmental cell, 18(4), 579–591. https://doi.org/10.1016/j.devcel.2010.03.007
26. Aapola, U., Kawasaki, K., Scott, H. S., Ollila, J., Vihinen, M., Heino, M., Shintani, A., Kawasaki, K., Minoshima, S., Krohn, K., Antonarakis, S. E., Shimizu, N., Kudoh, J., & Peterson, P. (2000). Isolation and initial characterization of a novel zinc finger gene, DNMT3L, on 21q22.3, related to the cytosine-5-methyltransferase 3 gene family. Genomics, 65(3), 293–298. https://doi.org/10.1006/geno.2000.6168.
27. Gowher, H., Liebert, K., Hermann, A., Xu, G., & Jeltsch, A. (2005). Mechanism of stimulation of catalytic activity of Dnmt3A and Dnmt3B DNA-(cytosine-C5)-methyltransferases by Dnmt3L. The Journal of biological chemistry, 280(14), 13341–13348. https://doi.org/10.1074/jbc.M413412200.
28. Zhang, Z. M., Lu, R., Wang, P., Yu, Y., Chen, D., Gao, L., Liu, S., Ji, D., Rothbart, S. B., Wang, Y., Wang, G. G., & Song, J. (2018). Structural basis for DNMT3A-mediated de novo DNA methylation. Nature, 554(7692), 387–391. https://doi.org/10.1038/nature25477.
29. Ooi, S. K., Qiu, C., Bernstein, E., Li, K., Jia, D., Yang, Z., Erdjument-Bromage, H., Tempst, P., Lin, S. P., Allis, C. D., Cheng, X., & Bestor, T. H. (2007). DNMT3L connects unmethylated lysine 4 of histone H3 to de novo methylation of DNA. Nature, 448(7154), 714–717. https://doi.org/10.1038/nature05987.
30. Messerschmidt, D. M., Knowles, B. B., & Solter, D. (2014). DNA methylation dynamics during epigenetic reprogramming in the germline and preimplantation embryos. Genes & development, 28(8), 812–828. https://doi.org/10.1101/gad.234294.113.
31. Guenatri, M., Duffié, R., Iranzo, J., Fauque, P., & Bourc'his, D. (2013). Plasticity in Dnmt3L-dependent and -independent modes of de novo methylation in the developing mouse embryo. Development (Cambridge, England), 140(3), 562–572. https://doi.org/10.1242/dev.089268.
32. Guttman, M., Donaghey, J., Carey, B. W., Garber, M., Grenier, J. K., Munson, G., Young, G., Lucas, A. B., Ach, R., Bruhn, L., Yang, X., Amit, I., Meissner, A., Regev, A., Rinn, J. L., Root, D. E., & Lander, E. S. (2011). lincRNAs act in the circuitry controlling pluripotency and differentiation. Nature, 477(7364), 295–300. https://doi.org/10.1038/nature10398.
33. Tu, C., Yang, K., Wan, L., et al. The crosstalk between lncRNAs and the Hippo signalling pathway in cancer progression. Cell Prolif. 2020;e12887. https://doi.org/10.1111/cpr.12887
34. Agarwal, V., Bell, G. W., Nam, J. W., & Bartel, D. P. (2015). Predicting effective microRNA target sites in mammalian mRNAs. eLife, 4, e05005. https://doi.org/10.7554/eLife.05005.
35. Napolitano, M., Comegna, M., Succoio, M., Leggiero, E., Pastore, L., Faraonio, R., Cimino, F., & Passaro, F. (2014). Comparative analysis of gene expression data reveals novel targets of senescence-associated microRNAs. PloS one, 9(6), e98669. https://doi.org/10.1371/journal.pone.0098669.
36. Dobin, A., Davis, C. A., Schlesinger, F., Drenkow, J., Zaleski, C., Jha, S., Batut, P., Chaisson, M., & Gingeras, T. R. (2013). STAR: ultrafast universal RNA-seq aligner. Bioinformatics (Oxford, England), 29(1), 15–21. https://doi.org/10.1093/bioinformatics/bts635.
37. Haeussler, M., Zweig, A. S., Tyner, C., Speir, M. L., Rosenbloom, K. R., Raney, B. J., Lee, C. M., Lee, B. T., Hinrichs, A. S., Gonzalez, J. N., Gibson, D., Diekhans, M., Clawson, H., Casper, J., Barber, G. P., Haussler, D., Kuhn, R. M., & Kent, W. J. (2019). The UCSC Genome Browser database: 2019 update. Nucleic acids research, 47(D1), D853–D858. https://doi.org/10.1093/nar/gky1095.
38. Li, B., & Dewey, C. N. (2011). RSEM: accurate transcript quantification from RNA-Seq data with or without a reference genome. BMC bioinformatics, 12, 323. https://doi.org/10.1186/1471-2105-12-323.
39. Robinson, M. D., McCarthy, D. J., & Smyth, G. K. (2010). edgeR: a Bioconductor package for differential expression analysis of digital gene expression data. Bioinformatics (Oxford, England), 26(1), 139–140. https://doi.org/10.1093/bioinformatics/btp616.
40. Afgan, E., Baker, D., Batut, B., van den Beek, M., Bouvier, D., Cech, M., Chilton, J., Clements, D., Coraor, N., Grüning, B. A., Guerler, A., Hillman-Jackson, J., Hiltemann, S., Jalili, V., Rasche, H., Soranzo, N., Goecks, J., Taylor, J., Nekrutenko, A., & Blankenberg, D. (2018). The Galaxy platform

for accessible, reproducible and collaborative biomedical analyses: 2018 update. Nucleic acids research, 46(W1), W537–W544. https://doi.org/10.1093/nar/gky379.
41. Testa, G., Russo, M., Di Benedetto, G., Barbato, M., Parisi, S., Pirozzi, F., Tocchetti, C. G., Abete, P., Bonaduce, D., Russo, T., & Passaro, F. (2020). Bmi1 inhibitor PTC-209 promotes Chemically induced Direct Cardiac Reprogramming of cardiac fibroblasts into cardiomyocytes. Scientific reports, 10(1), 7129. https://doi.org/10.1038/s41598-020-63992-8.
42. Krueger, F., & Andrews, S. R. (2011). Bismark: a flexible aligner and methylation caller for Bisulfite-Seq applications. Bioinformatics (Oxford, England), 27(11), 1571–1572. https://doi.org/10.1093/bioinformatics/btr167.
43. Akalin, A., Kormaksson, M., Li, S., Garrett-Bakelman, F. E., Figueroa, M. E., Melnick, A., & Mason, C. E. (2012). methylKit: a comprehensive R package for the analysis of genome-wide DNA methylation profiles. Genome biology, 13(10), R87. https://doi.org/10.1186/gb-2012-13-10-r87.
44. Akalin, A., Franke, V., Vlahoviček, K., Mason, C. E., & Schübeler, D. (2015). Genomation: a toolkit to summarize, annotate and visualize genomic intervals. Bioinformatics (Oxford, England), 31(7), 1127–1129. https://doi.org/10.1093/bioinformatics/btu775

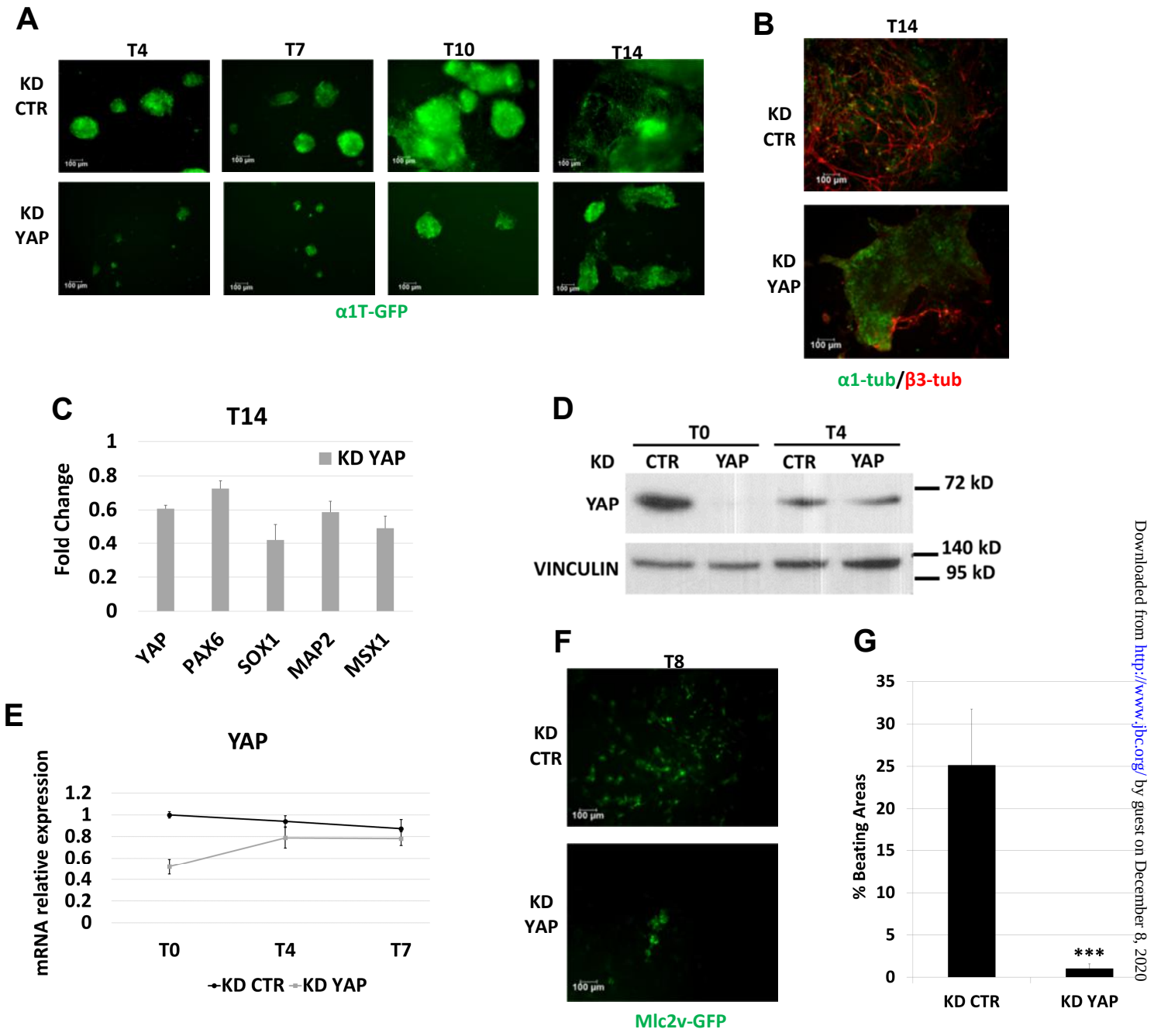

Figure 1. Transient knockdown (KD) of Yap impairs ESCs differentiation.
(A) α1T-GFP stable cell line transfected with Stealth siRNA to silence YAP expression (KD YAP) showed a decrease in neuroectodermal differentiation efficacy with respect to KD control (KD CTR) cells. Representative images are shown. Scale bar: 100μm. **(B)** Representative immunostaining of neural marker β3-tubulin (red) in α1T-GFP (green) at final stage (T14) of differentiation showing a dramatic reduction in post-mitotic neuronal differentiation. Scale bar: 100μm. (**C**) qPCR analysis of neuronal marker gene expression upon differentiation of YAP KD cells. Data are shown as Fold Changes with respect to KD CTR cells. *p<0.05, **p<0.01. (**D**) YAP expression profile over neuroectodermal differentiation by Western blot or (**E**) qPCR. (**F**) YAP KD in mlc2v-GFP stable cell line showed a strong reduction of mesodermal differentiation efficiency compared to KD CTR cells. Representative immunostainings are shown. Scale bar: 100μm. (**G**) Percentage of beating areas at final stage of differentiation (T8), demonstrating a significant (***p<0.01) decrease in mature cardiomyocytes generation upon YAP KD. For each data set, averaged numbers from biological triplicates were used for statistics. Error bars indicate mean ± SEM.

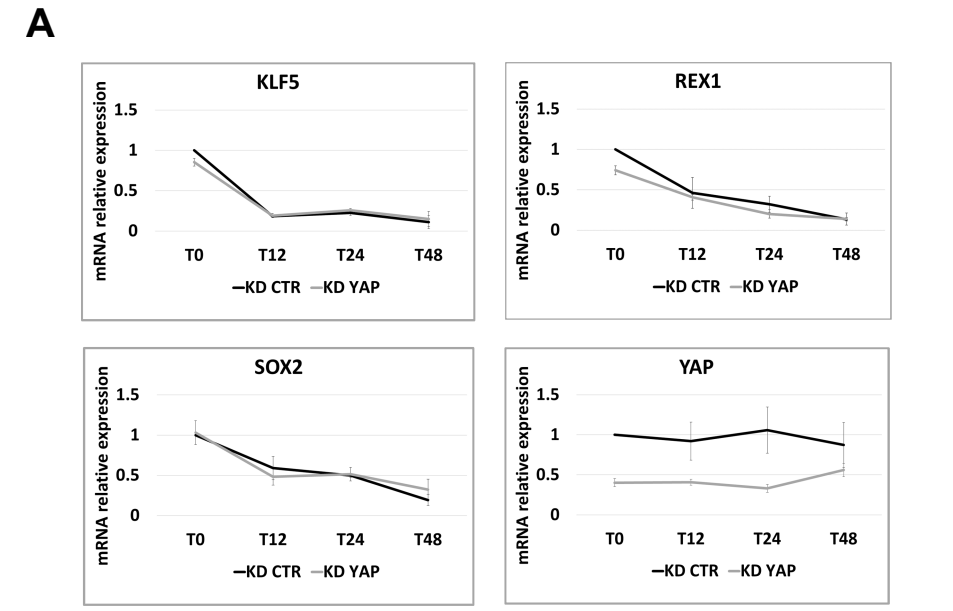

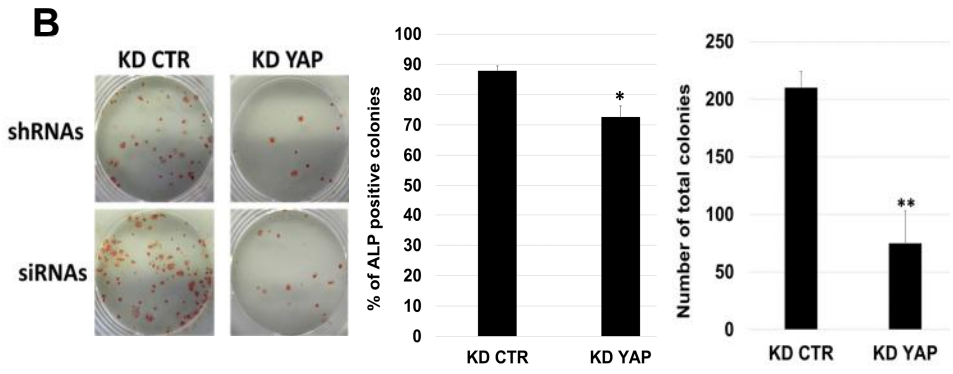

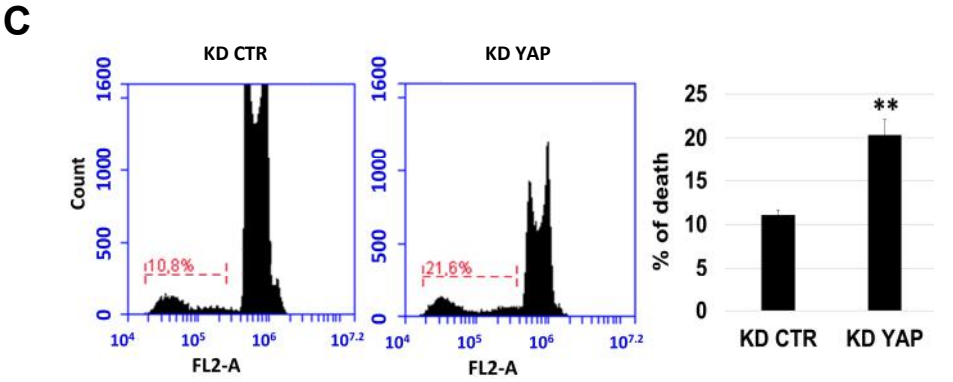

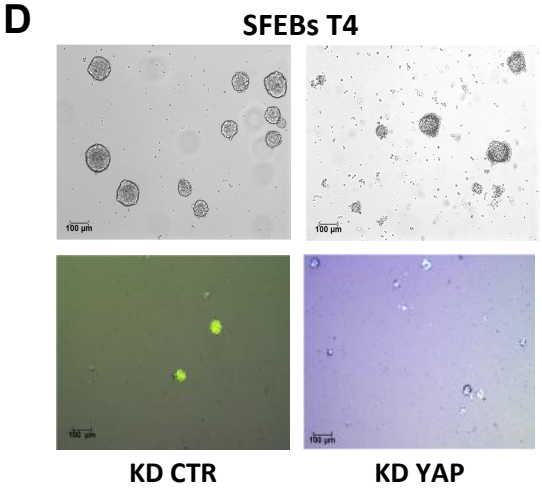

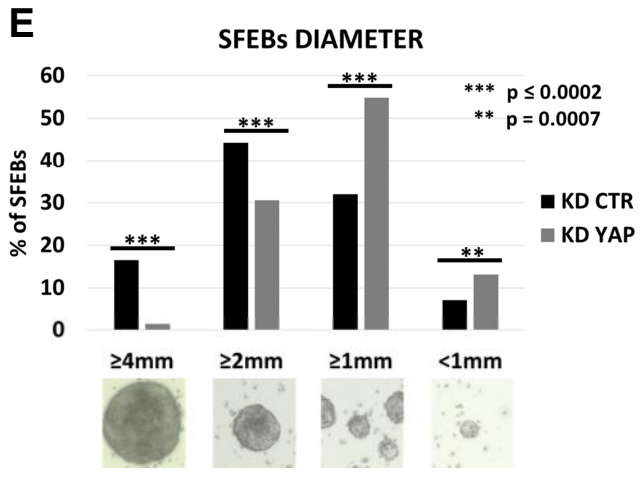

Figure 2. The KD of YAP does not impair ESCs pluripotency but decreases cell viability.

(A) qPRC analysis of stemness marker genes upon LIF withdrawal in KD YAP compared to KD CTR cells. For each data set, n=3. Error bars indicate mean ± SEM. **(B)** Representative images of Alkaline Phosphatase (AP) staining at day 7 upon siRNAs transfection. YAP KD causes a significant (**p<0.01) decrease in the number of total AP colonies, whereas the percentage of AP positive colonies seems to be almost unaffected (*p<0.05) with respect to CTR KD cells. For each data set, n=3. Error bars indicate mean ± SEM. **(C)** Representative flow-cytometry histograms of gated nuclei fluorescence (propidium iodide staining) detected using the FL2 (480 nm) photodetector (FL2-A). YAP KD significantly (**p<0.01) increases the percentage of sub G0/G1 cell population, compared to KD CTR. n=3, Error bars indicate mean ± SEM. **(D)** Representative images of KD CTR and KD YAP SFEBs tested with Trypan Blue exclusion assay Scale bar: 100 µm.

(E) Statistical analyses of Serum Free Embryo Bodies (SFEBs) dimensions from YAP KD compared to CTR KD cells. Diameter measurement was performed using ImageJ 1.52v software. For each data set, 300 SFEBs from each biological triplicate were analyzed. Error bars indicate mean ± SEM.

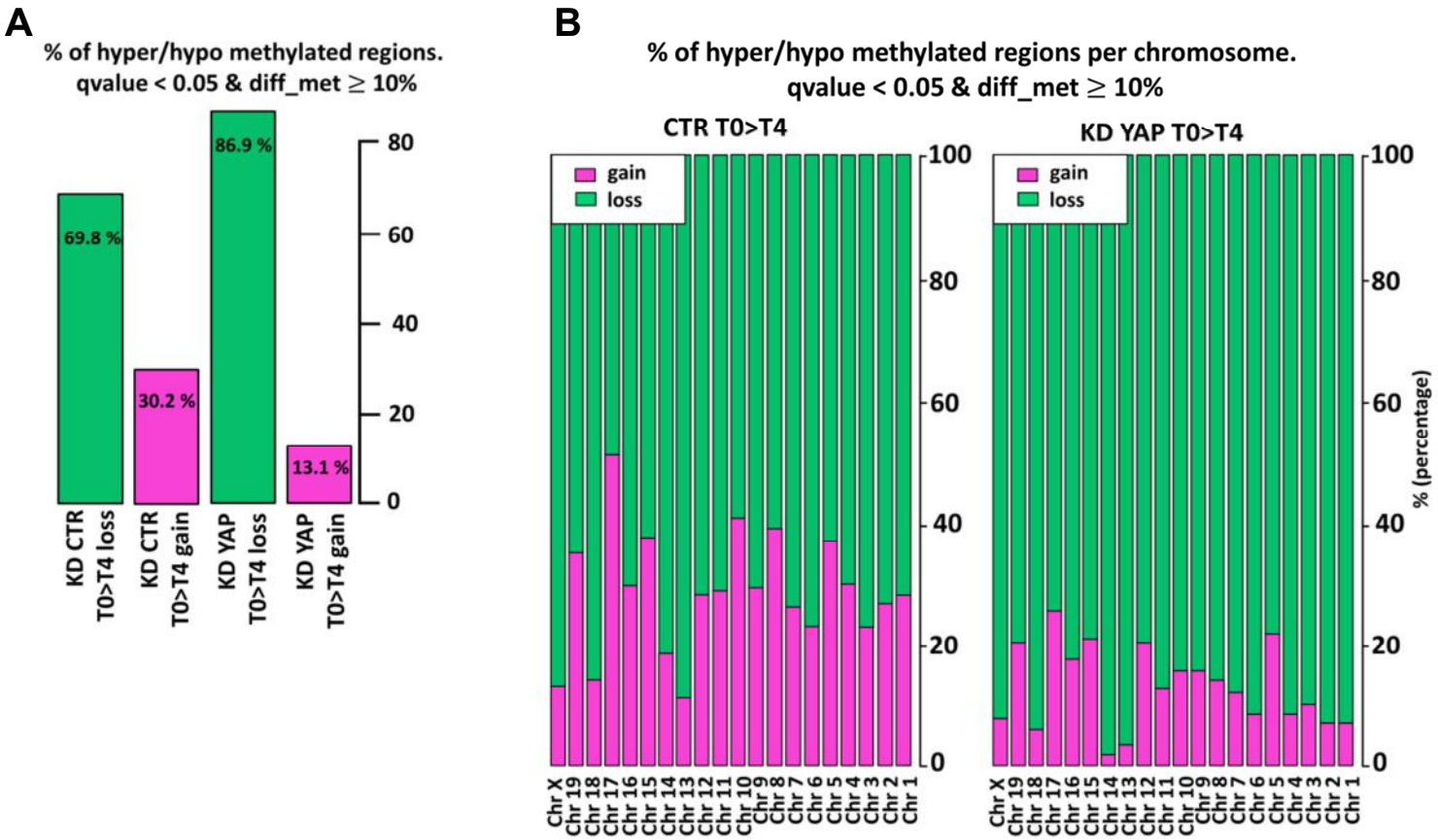

C

PANTHER Pathways	Fold Enrichment	raw P-value	FDR
Cadherin signaling pathway (P00012)	3.94	3.74E-11	2.07E-09
Wnt signaling pathway (P00057)	2.92	2.24E-11	1.86E-09
Heterotrimeric G-protein signaling pathway-Gi alpha and Gs alpha mediated pathway (P00026)	2.61	4.72E-05	1.96E-03
Gonadotropin-releasing hormone receptor pathway (P06664)	2.1	3.32E-04	1.10E-02

Figure 3. BS-seq revealed an imbalance in the methylation pattern of YAP KD cells.
(A) Analysis of DMRs at day 4 (T4) of SFEBs differentiation compared to undifferentiated (T0) cells. Histograms represent the percentage of global loss (green bar) and gain (pink bar) of methylated regions measured in CTR or YAP KD cells, with a qvalue cutoff < 0.05 and a differential methylation cutoff > 10%. **(B)** Analysis of DMRs distribution per chromosome. Histograms represent the percentage of loss (green bar) and gain (pink bar) of methylated regions per chromosome measured in CTR KD and in YAP KD cells at T4 of SFEBs differentiation. qvalue < 0.05 and differential methylation > 10%. **(C)** Functional enrichment analysis for significantly over-represented pathways (FDR < 0.05) among genes showing a loss of methylation upon YAP KD cells at T4 of SFEBs differentiation, according to Panther.

A

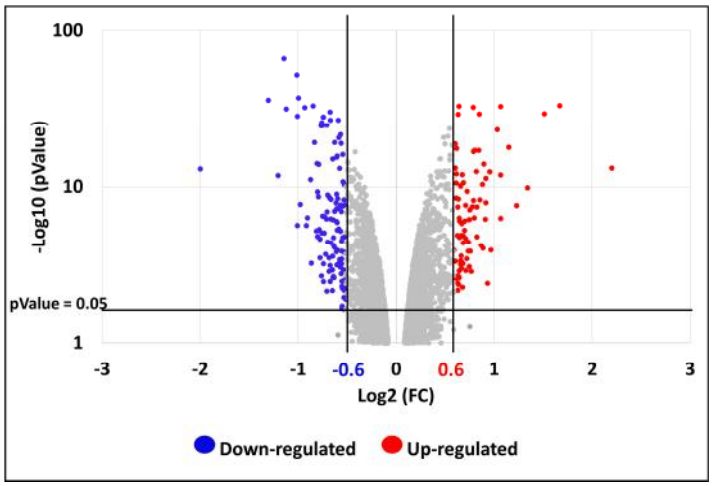

B

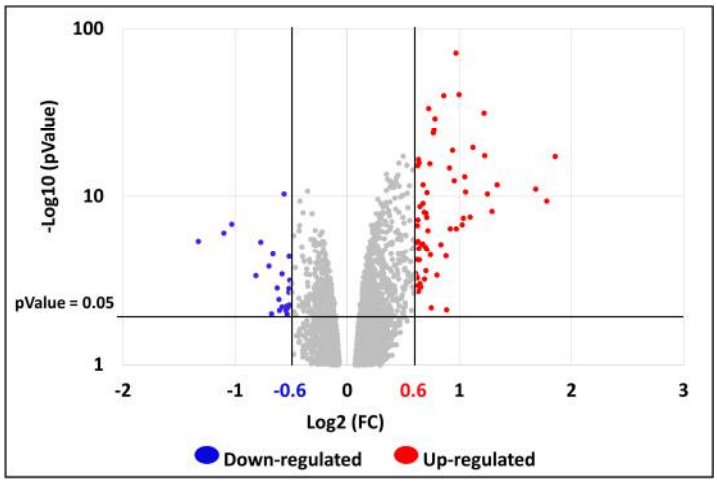

C

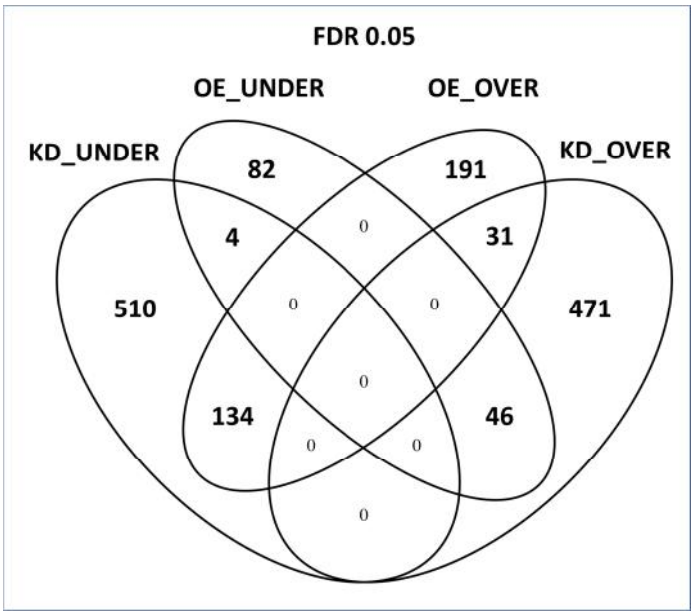

D

GO TERMS	BIOLOGICAL PROCESS	FDR
GO:0045823	positive regulation of heart contraction	1.08E-02
GO:0060425	lung morphogenesis	2.65E-02
GO:0001894	tissue homeostasis	2.68E-02
GO:0048871	multicellular organismal homeostasis	9.87E-03
GO:0007267	cell-cell signaling	7.57E-03
GO:0050767	regulation of neurogenesis	1.72E-02
GO:0022603	regulation of anatomical structure morphogenesis	1.12E-02
GO:0051960	regulation of nervous system development	2.02E-02
GO:0060284	regulation of cell development	2.45E-02
GO:2000026	regulation of multicellular organismal development	1.86E-03
GO:0048699	generation of neurons	1.66E-02
GO:0009888	tissue development	2.63E-02
GO:0022008	neurogenesis	1.58E-02
GO:0009653	anatomical structure morphogenesis	1.02E-02
GO:0007399	nervous system development	1.14E-02
GO:0050793	regulation of developmental process	9.39E-03
GO:0030154	cell differentiation	7.73E-03
GO:0048731	system development	4.36E-03
GO:0048869	cellular developmental process	8.37E-03
GO:0051239	regulation of multicellular organismal process	4.30E-02
GO:0007275	multicellular organism development	6.54E-03
GO:0048856	anatomical structure development	5.59E-03
GO:0032502	developmental process	4.89E-03

Figure 4. Gene expression profile of YAP KD cells.
(A) Volcano plot for differentially expressed genes (DEGs), which revealed 1196 DEGs in KD YAP cells compared to KD CTR. The negative log of pValue (base 10) is plotted on the Y-axis, and the log of the FC (base 2) is plotted on the X-axis. Red plots represent significant (pValue<0.05) and remarkable (FC>1.5) upregulated genes, while blue plots represent significant (pValue< 0.05) and remarkable (FC<0.7) downregulated genes. **(B)** Volcano plot showing 488 DEGs in OE YAP cells compared to OE CTR. The negative log of pValue (base 10) is plotted on the Y-axis, and the log of the FC (base 2) is plotted on the X-axis. Red plots represent significant (pValue<0.05) and remarkable (FC>1.5) upregulated genes, while blue plots represent significant (pValue< 0.05) and remarkable (FC<0.7) downregulated genes. **(C)** Venn diagram showing the number of common and unique genes, upregulated (OVER) and downregulated (UNDER), in YAP KD (KD) and YAP OE (OE) cells. **(D)** Panther functional enrichment analysis of the most deregulated genes (0.6 < FC > 1.7) in YAP KD for significantly over-represented Biological Process (FDR < 0.05).

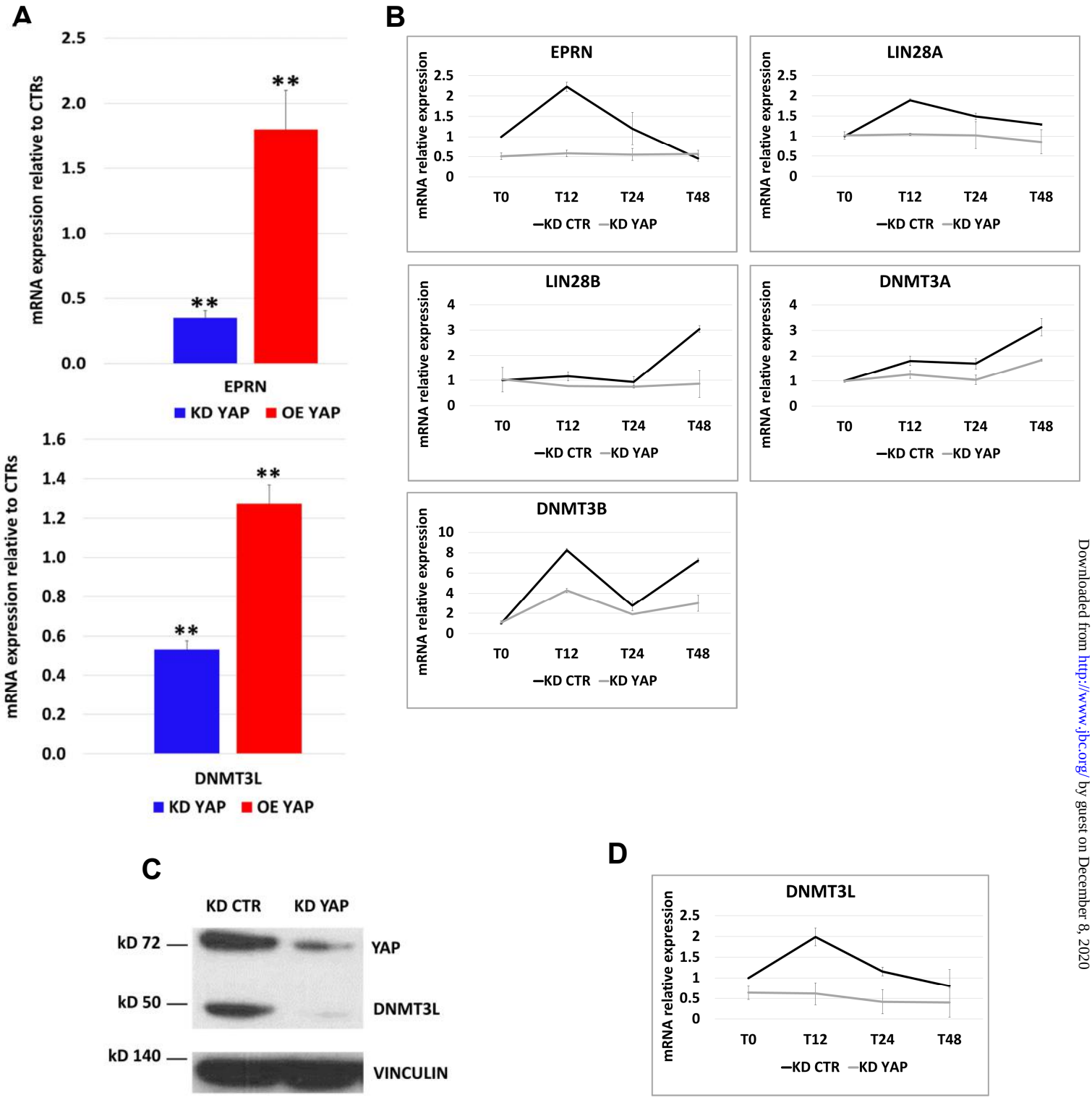

Figure 5. YAP regulates Eprn and Dnmt3l gene expression.
(**A**) Validation by qPCR analysis of Eprn and Dnmt3l expression upon YAP KD or YAP OE, with respect to CTR cells. For each dataset n=3. Error bars indicate mean ± SEM. **(B)** Gene expression profile of Eprn, Lin28a, Lin28b, Dnmt3a and Dnmt3b in YAP KD cells at different time points (T0-T12-T24-T48 hours) upon LIF withdrawal. For each dataset n=3. Error bars indicate mean ± SEM. Data are reported with respect to gene expression profile in KD CTR cells at same time of differentiation. **(C)** Representative Western Blot showing the downregulation of Dnmt3l at protein level upon 48h of YAP KD. **(D)** Gene expression profile of Dnmt3l in YAP KD cells at different time points (T0-T12-T24-T48 hours) upon LIF withdrawal. For each dataset n=3. Error bars indicate mean ± SEM. Data are reported with respect to gene expression profile in KD CTR cells at same time of differentiation.

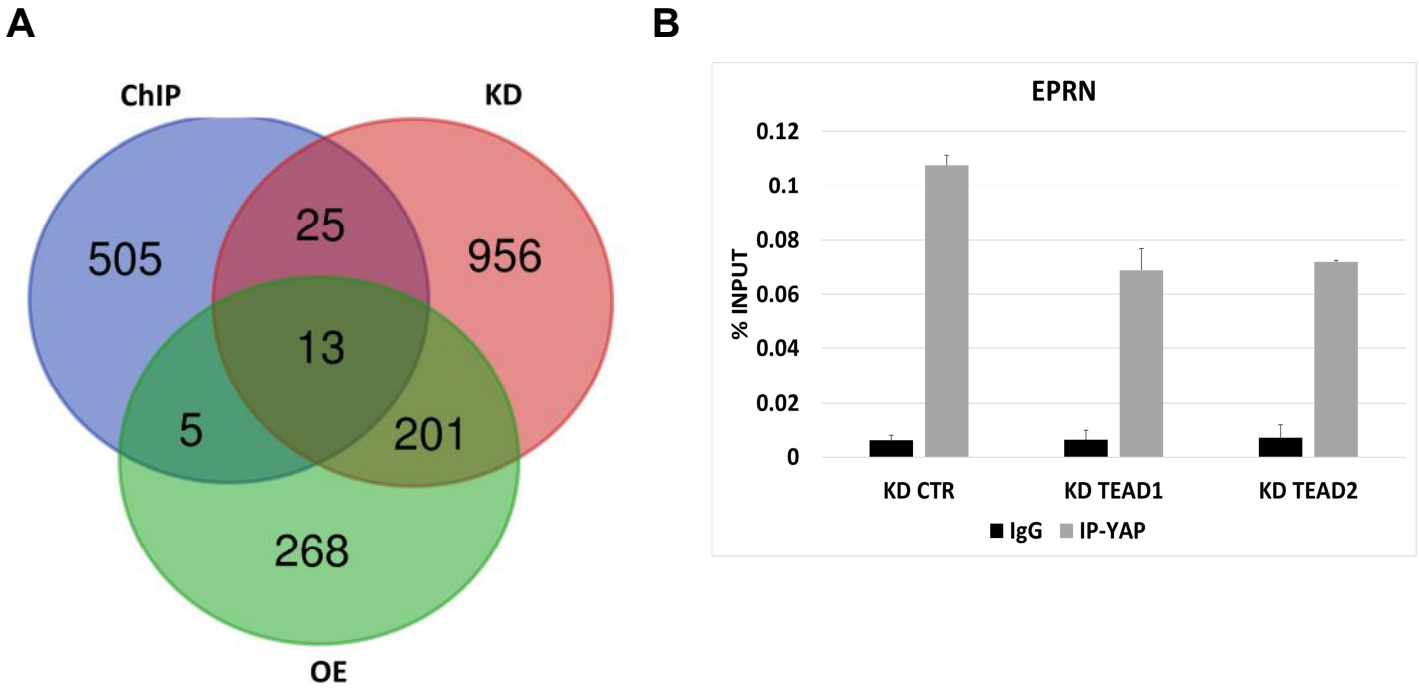

Figure 6. Eprn is a direct target of YAP/TEAD2.
(A) Venn diagram showing the number of common and unique genes among YAP KD (KD), YAP OE (OE) and YAP ChIP-seq (ChIP). **(B)** ChIP-qPCR for YAP on Eprn locus in KD CTR, KD TEAD1 and KD TEAD2 cells. Data are showed as % of precipitated DNA, calculated relative to the total input chromatin and expressed as the fold enrichment relative to total input. Averaged numbers from biological duplicates were used for statistics.

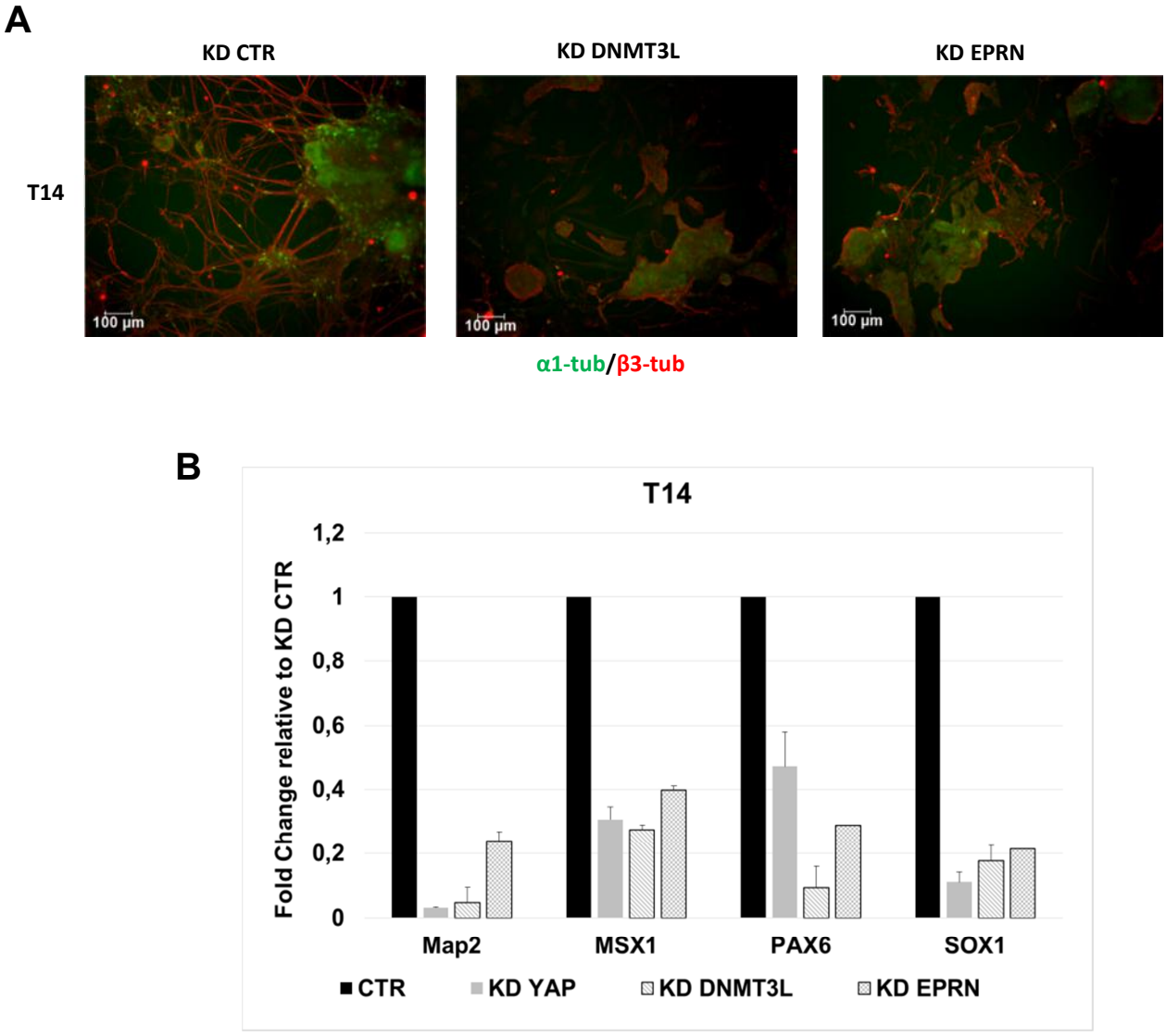

Figure 7. Eprn and Dnmt3l KD affect ESCs differentiation.
(**A**) α1T-GFP stable cell line transfected with Stealth siRNA to silence YAP (KD YAP), DNMT3L (KD DNMT3L) or EPRN (KD EPRN) expression showed a decreased in neuroectodermal differentiation with respect to KD control (KD CTR) cells. Representative immunostaining of neural marker β3-tubulin (red) in α1T-GFP (green) cells at final stage (T14) of differentiation are shown. Scale bar: 100µm. **(B)** qPCR analysis of neuronal marker gene expression upon differentiation of KD cells. Data are shown as Fold Changes with respect to KD CTR cells. For each data set, n=2. Error bars indicate mean ± SEM.

YAP contributes to DNA methylation remodeling upon mouse embryonic stem cell differentiation

Fabiana Passaro, Ilaria De Martino, Federico Zambelli, Giorgia Di Benedetto, Matteo Barbato, Anna Maria D'Erchia, Caterina Manzari, Graziano Pesole, Margherita Mutarelli, Davide Cacchiarelli, Dario Antonini, Silvia Parisi and Tommaso Russo

J. Biol. Chem. published online December 2, 2020

Access the most updated version of this article at doi: 10.1074/jbc.RA120.015896